Experimental detection of terahertz radiation in bundles of single wall carbon nanotubes

K.S. Yngvesson, K. Fu, B. Fu, R. Zannoni, J. Nicholson, S.H.Adams, A. Ouarraoui, J. Donovan and E. Polizzi

Department of Electrical and Computer Engineering,

University of Massachusetts, Amherst, MA 01003, USA

* Contact: yngvesson@ecs.umass.edu; phone +01-413-545-0771

***Abstract*— We present new data extending our previous paper at the ISSTT2006 on microwave detection in carbon nanotubes (CNTs). In particular, we derive a circuit model based on ANA measurements. We also demonstrate the first terahertz detection (up to 2.54 THz) in bundles of CNTs that were deposited through dielectrophoresis across the smallest gap in log-periodic antennas. Data are given that support the hypothesis that the detection process is bolometric at THz frequencies. Future extensions are planned that will employ suspended CNTs and explore heterodyne detection. Finally, we have performed unique ab initio simulations with the aim of comparing these with the experimental data.**

I. INTRODUCTION

Our paper at the **ISSTT2005** [1] posed the question: Can we make a carbon nanotube (CNT) THz HEB? We also discussed this topic in ref. [2]. At the **ISSTT2006** we presented results of microwave (MW) direct and heterodyne detection in *metallic* single wall carbon nanotubes (m-SWCNTs) [3,4]. Other groups have also demonstrated MW detection in SWNTs, primarily in *semiconducting* tubes (s-SWCNTs) [5-9]. McEuen et al. [10] used THz time-domain techniques for detection in a quasi-metallic (qm) SWCNT FET type device. Photoconductive detection in SWCNTs is apparently very weak [11], but Itkis et al. [11] have developed a sensitive *bolometric* Near Infrared detector based on a Carbon Nanotube (CNT) film. We recently reported the first terahertz detection in bundles containing m-SWCNTs [12], up to 2.5 THz. The present paper gives further results for this detector [13]. In particular, we have characterized the devices at microwave frequencies, and we also interpret the experimental terahertz detection based on a general bolometric model.

As we discussed in ref. [1-2] CNTs are a promising medium for future terahertz bolometric detectors (HEBs or other types) based on some general features:

(1) SWCNTs have diameters of only about 1-2 nm and typical lengths of ~ 1 μm. Consequently, they have lower heat capacity than for example NbN HEBs, which is advantageous for low local oscillator power.
(2) SWCNTs have excellent thermal transport properties, including ballistic transport of both phonons and electrons in the shorter tubes. Based on (1) and (2) we can predict that SWCNT bolometric detectors can potentially have very short thermal time constants, translating into very wide bandwidth for heterodyne detectors.
(3) SWNT detectors are not restricted to working below a critical temperature as are superconducting HEBs. There is thus a potential for operation above 4 K.

II. DEVICE FABRICATION

In this work, we used nonconductive sapphire or silicon on sapphire (SOS) substrates. The choice of these substrates was crucial for both MW and THz measurements. In our previous MW work [3,4] we employed highly doped silicon substrates with a thin coating of silicon oxide, a common choice in many SWNT investigations since it allows application of a gate voltage to the substrate. Metallic and semiconducting tubes can then be conveniently distinguished due to the different effects the gate voltage has on their resistance. As a consequence of the use of the conducting substrate in our previous work, however, the MW detection responsivity dropped quickly above about 1 GHz. Further, the doped silicon substrates attenuate the THz radiation very strongly, while sapphire and SOS substrates show very low THz attenuation. The sapphire and SOS substrates were found to be equivalent in our work.

We fabricated the m-SWCNT devices by the dielectrophoresis (DEP) method [14]. Typically, we apply a 5 - 50 MHz voltage of about 5 V peak to Au contacts made by UV photolithography, such as those shown in Figures 1 and 2. To the left is a coplanar waveguide (CPW) structure that we used for MW measurements. It has a gap of about 4-6 μm. For THz measurements we employed a log-periodic toothed antenna (LPA1) with about an 8 μm gap, as shown to the right in Figure 1. LPA 1 has an estimated upper frequency limit of 1.5 THz. We also fabricated LPAs with a smaller gap, about 1 μm (LPA2), as well as smaller teeth, see Figure 2. LPA 2 has an estimated upper frequency limit of 3.5 THz.

A drop of a suspension of CNTs in isopropyl alcohol [15] was applied to these structures. The CNTs will then drift to the narrow gap in the contacts and attach to these, when the

RF voltage is applied across the contacts. We monitor the DC resistance simultaneously through a bias tee. The DEP process is halted when the dc resistance is sufficiently low. All devices were annealed in air at 200 °C for two hours which decreased the contact resistance. The result is that a small number of bundles of CNTs will be contacted in parallel across the gap. The lower resistance of these devices compared with the typical single SWCNTs, from 5 to 50 kΩ, facilitates matching of microwaves or terahertz radiation to the CNTs. While semiconducting tubes are expected to be present in the bundles, we assume these to have a negligible effect at dc compared with metallic tubes, due to the known much higher resistance of the former. A typical IV-curve is shown in Figure 3. The IV-curve displays the same "zero-bias anomaly" [16] that we had previously observed for the single m-SWNTs (as versus bundles) in ref. [3,4]. Figure 3 also shows dI/dV, which has a minimum at zero bias. The nonlinearity of the IV-curves is more pronounced the lower the temperature is. We conclude that the IV-curves are due to a number of parallel metallic tubes in the bundles.

Figure 1. Microwave CPW (left) and terahertz LPA1 (right) structures for coupling to the CNTs.

Figure 2. LPA2 with 1 μm gap used in later THz measurements.

III. Microwave Measurements

A. Microwave S11 Measurements

Both structures in Figure 1 can be measured in a microwave probe system, a useful diagnostic tool. Most of our MW measurements were performed on the CPW structure. Each tube is assumed to be modeled by the equivalent circuit introduced and analyzed by P. Burke [17], see Fig. 4. The *m*-SWCNT at the center of Fig. 4 is modeled as a transmission line (TL), and the unit cell shown is repeated periodically. The propagation velocity on the TL (v_P) is about 0.01 times the velocity of light ($2.4*10^6$ m/s), interpreted as the velocity of a "Tomonaga–Lüttinger plasmon" wave.

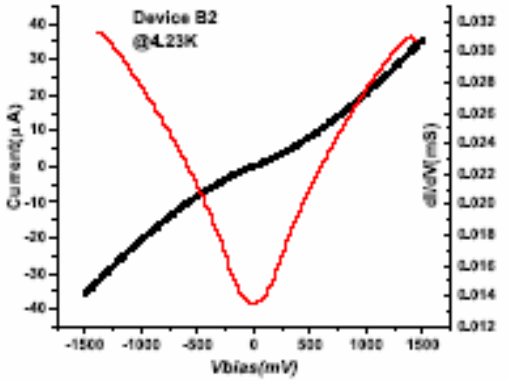

Figure 3. IV-curve (in black) for one of the devices, measured at 4.2 K. Also shown is dI/dV derived from this curve (in red). The left scale gives the current in μA and the right scale dI/dV in mS.

It is predicted that resonances will occur on the TL at terahertz frequencies for which its electrical length is a multiple of half wavelengths. The characteristic impedance (Z_c) of the TL is 9.7 kΩ. In later work, Hanson [18] and Maksimenko et al. [19] have taken into account the electromagnetic fields *outside* the CNT and find v_P about twice that of [17], as well as modified TL parameters for bundles of CNTs [19]. Very recently, McEuen et al. [10] measured the ballistic electron resonance in quasi-metallic (qm) SWCNTs and found that in their experiment v_P was that of single particle excitations (i.e. the Fermi velocity, $8*10^5$ m/s). These issues are thus presently under debate and need to be settled through further measurements at THz frequencies. At MW frequencies, however, the SWCNTs are much shorter than a wavelength, and it suffices to model the SWCNT as an inductance (the kinetic inductance, L_K) and a resistance (R_{CNT}) in series. The contacts were modeled by a resistance (R_C) in parallel with a capacitance (C_C). The capacitance to ground from the CNT has a negligible effect and could be omitted.

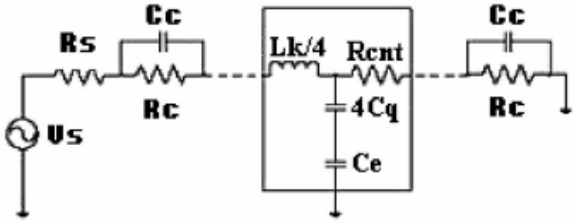

Figure 4. Equivalent circuit model for a m-SWNT.

Each substrate fabricated had a large number of CPW structures. The S-parameter S11 was measured for frequencies up to 26 GHz after calibration with a standard substrate up to the reference plane of the probe (Hewlett-Packard ANA 8510C). The admittance was then calculated from S11. We used DEP to place CNTs across the gaps of

only a few of the CPWs, and the rest could be used as references in a de-embedding process in which the admittance of the circuit *without CNTs* was subtracted from that of the circuit *with CNTs*. Using this procedure we thus obtained the admittance of the CNTs by themselves. The de-embedded data were then fitted to the circuit model, and this procedure was successful over the full frequency range for three out of four devices. The fourth device (device C) only gave a good fit to about 3 GHz. We expected some variability in the device data due to the fact that we could not control the DEP process completely. Table 1 below summarizes the circuit parameters we derived from the S11 measurements. The values for the resistances are consistent with typical CNT resistances *per m-SWCNT* of about 10 kΩ/μm at 300 K [20] and typical (total) contact resistances of the order of 500 - 1000 kΩ, if we assume that we have 100 tubes in parallel. The theoretical value for L_K is 4 nH/μm [17] and we would expect to measure a value of 0.01-0.02 nH for 100 tubes, about 4 μm long, in parallel. Our measurements are consistent with this if we take into account that our accuracy in estimating the inductance was marginal, except to determine that it is small. Note that Device C did not yield a good fit, and may have a different structure. Two recent measurements by other researchers (ref. [21,22]) estimated L_K for a single m-SWCNT and a small number of tubes (15) in parallel, respectively, but with fairly large error bars. All attempted measurements of L_K are consistent with the theory, so far, however. All measurements so far also show a significant contact capacitance, similar to our results that range from 4 fF to 40 fF. We will return to a discussion of the contact capacitance in the THz section. A typical result of the fit to the model is shown in Figure 5.

TABLE I.
PARAMETER VALUES FOR THE CIRCUIT MODEL FITS TO THE MEASURED S11 DATA.

Device	R_{CNT} (kΩ)	L_K (nH)	R_{C1} (kΩ)	R_{C2} (kΩ)	C_{C1} (fF)	C_{C2} (fF)
C	0.34	92	1.94	1.52	2	42
D	0.08	2.50	4.28	4.73	4.96	4.50
E1	0.29	0.03	1.06	7.29	23.4	21.6
F	0.20	0.05	0.61	3.25	32.4	37.5

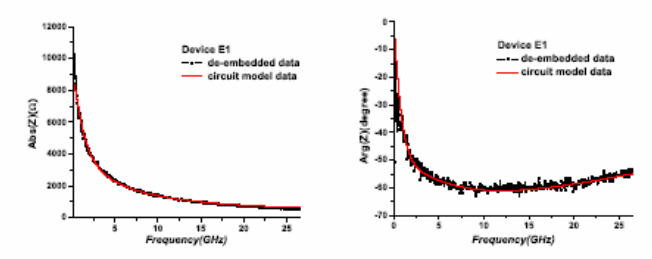

Figure 5. Best fit of the de-embedded data for the measured values of ABS(Z) (ohms) (left) and ARG(Z) (degrees) (right) of Device E1 (black points), compared with the model (red line).

B. Microwave Detection Measurements

We dc biased CNT devices that were contacted by the microwave probes, by feeding the current from a programmable Source Meter (Keithley 2400) through a bias tee. We then fed microwave power, modulated at 1 kHz, to the devices and detected the change in the dc current with a lock-in amplifier. The microwave power was measured with a power meter. The circuit connections were similar to what was used in the THz experiments and will be presented later. Five devices were measured. Figure 6 shows the detected responsivity versus bias voltage for one of these. This curve shows a reasonable fit to the predicted response (see below). The fit is not as good as for the single tubes measured in our earlier work [3,4], as would be expected based on the more complex structure of the bundles. It is also broader, and another difference is that the maximum responsivity is much larger (from 600 V/W to 1,000 V/W, compared with 114 V/W). The responsivity in [3,4] was measured at 77 K, whereas the new results are at room temperature. Clearly, devices containing SWNT bundles are superior to the single tube devices that were employed for the earlier measurements. The responsivity is defined as

$$S_V = \Delta V / P_{MW} = S_I * R \qquad (1)$$

$$S_I = (1/4)*(d^2I/dV^2)*V^2_{MW}/P_{MW} \qquad (2)$$

Here, ΔV is the detected change in dc voltage, V_{MW} is the peak MW voltage and P_{MW} is the MW power. As in [3,4] we derive the voltage responsivity from $R*(d^2I/dV^2)$, which was obtained from the measured IV-curves, in the same manner as for a standard microwave detector diode [22]. Note from Table 1 that the contact resistance is much larger than the actual CNT resistance, i.e. the nonlinearity of the IV curve can be ascribed to the contact resistance.

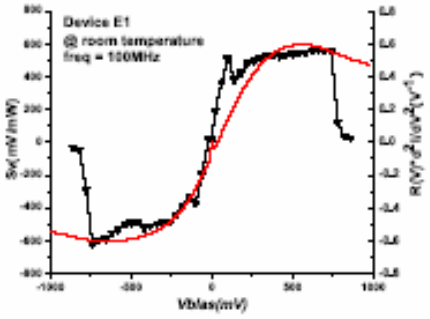

Figure 6. Voltage responsivity (S_V) for device E1 at a frequency of 100 MHz, versus bias voltage (black points) compared with the prediction based on Eq's (1) and (2).

Finally we measured the voltage responsivity as a function of MW frequency, see Figure 7. The effect of parasitics was partly avoided by calibrating the microwave power at the probe. The small drop in responsivity as the frequency is increased is consistent with a prediction based on the circuit model [13]. It is due to the contact capacitance beginning to shunt the contact resistance, which makes the detector less effective. We conclude that in this mode of detection (the

"diode mode") the detector has a high responsivity up to a few tens of GHz, with a cut-off frequency that depends on the value of the contact RC time constant.

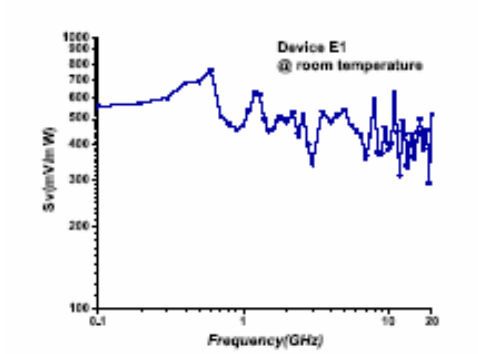

Figure 7. Frequency dependence of the maximum S_V for Device E1.

IV. TERAHERTZ MEASUREMENTS AND MODELING

A. THz Measurement Setup

For the terahertz measurements, a device chip with dimensions 6x6 mm^2 was inserted in a fixture (Figure 8) available from our earlier work with NbN HEB receivers [24]. The fixture allowed quasi-optical coupling to terahertz radiation, as well as bias input and detector output through a coaxial cable and a bias tee. Gold bond wires were used to connect to the contact pads of the LPA shown in Figure 1 (right). The LPA in Figure 2 has a larger contact area, shaped like a CPW, and we were able to connect it with indium wire. The fixture was then mounted in a liquid helium dewar.

A 4 mm diameter ellipsoidal silicon lens was attached to the substrate for quasi-optical coupling to the antenna as shown in Fig. 9.

Figure 8. The fixture used for THz measurements. The device chip is in the center of the fixture and the silicon lens on the opposite side (visible through the sapphire substrate).

A 100 kΩ resistor is connected in series with the carbon nanotube, and the Keithley Source Meter is connected directly to the resistor. The dc voltage across the two terminals of the carbon nanotubes is sensed at the V_{sense} port. The Source Meter also measures the current through the carbon nanotubes. A change in the device current gives rise to a voltage drop across the 100 kΩ resistor that is measured with a lock-in amplifier (EG&G 7260), which has an input impedance of 1 MΩ, through two 200 kΩ resistors. A 1 kHz signal from a function generator was employed as reference for the lock-in amplifier.

Terahertz radiation was introduced through the dewar window and the silicon lens from a CO_2-laser (Coherent/DEOS GEM-50) pumped terahertz gas laser that had a typical output power of 2-5 mW (Figure 11). The power could be measured with a Scientech (Astral AA30) power meter. The laser was modulated from the same 1 kHz function generator by inserting an acousto-optic modulator (IntraAction AGM-406B21) after the CO_2 pump laser, as indicated in Figure 10.

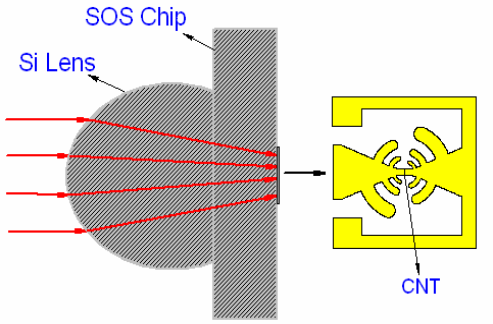

Figure 9. The quasi-optical coupling configuration.

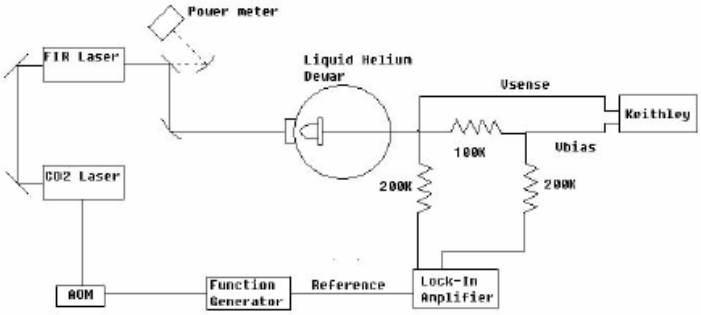

Figure 10. THz measurement setup.

Figure 11. The CO_2-laser pumped THz gas laser

B. Overview of Experimental THz Results

Using the configuration described in section IV.A we have demonstrated detection in CNT bundles at five different frequencies (0.694 THz, 1.05 THz, 1.39 THz, 1.63 THz and 2.54 THz). We measured the response for five devices of quite different resistances, see Table II. The resistance values given are for 300 K and low bias voltage.

Device B initially had a room temperature resistance of 7 kΩ ("Device B1") which after about one month changed to 20 kΩ ("Device B2"). Many experiments were then performed on Device B2 during which the IV-curves at a given temperature stayed the same.

TABLE II.

Device	Resistance (kΩ)	Antenna	# Active m-SWNTs
A	430	LPA1	3-5
B1	7	LPA1	50
B2	20	LPA1	50
1μmB2	65	LPA2	5
1μmC3	3	LPA2	50

A summary of all terahertz detections obtained so far is given in Figure 12. The terahertz power was measured outside the window of the dewar, and the response was linear in power. There is a roughly 3 to 4 dB optical loss between the dewar window and the antenna terminals. It is clear that there is a general type of detection process that works for a wide range of terahertz frequencies. There appears to be a pattern of decreasing responsivity from 0.694 THz to 1.63 THz, but the responsivity then increases at 2.54 THz, in contradiction to that trend. The higher resistance device A has more than an order-of-magnitude lower responsivity than Device B2.

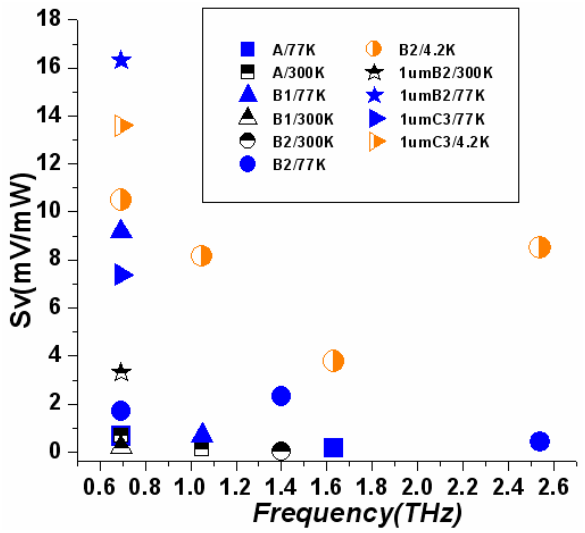

Figure 12. Summary of measured THz responsivity versus frequency.

Some devices show no or only very weak detection at 300 K, but Device 1μmB2 is an exception to this rule. We first discuss the results for Device B2 in detail.

C. *The Bolometric Model*

We measured the bias voltage dependence of the voltage responsivity for all devices in order to test the hypothesis that the detection process for the new THz detector is bolometric, as had been found for the IR CNT film detector in ref. [11]. A block diagram of a general bolometer is given in Figure 13. A bolometer is a device that has a temperature-dependent resistance R(T) and a heat capacity C_h. The bolometer is thermally connected through a thermal conductance G_{th} to a heat reservoir at temperature T_0.

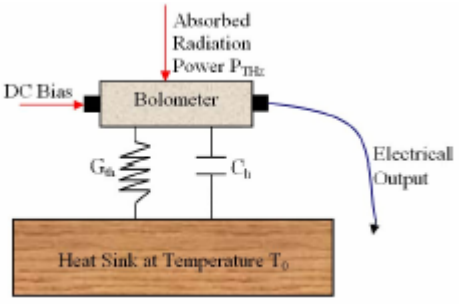

Figure 13. A bolometer model.

As the bolometer is heated by the terahertz power and biased by the dc current I_0, its temperature is increased from T_0 to $T_0 + \Delta T$. If we define the factor $b = (1/R)*dR/dT$ then the voltage responsivity of the bolometer will be (neglecting electro-thermal feedback) [25]:

$$S_V = \Delta V/P_{THz} = \frac{I_0 * R * b}{[G_{th} + i\omega C_h]} (V/W) \qquad (3)$$

The thermal time-constant of the bolometer is determined by $\tau_{th} = C_h/G_{th}$.

In Sec. III A we found that the contact capacitance (C_C in the equivalent circuit in Figure 4) has values ranging from 4 fF to 40 fF, large enough that it effectively shunts the contact resistance at THz frequencies. We estimate that Device B2 may have about 50 ("active") metallic SWCNTs in parallel. Simulation of the circuit in Figure 4 (for a single m-SWCNT) shows that the mismatch loss right at the resonance frequencies may have large peaks, if the damping is weak [17]. We have simulated Device B2 using parameters for the circuit model such as Z_C and v_P based on [17], while varying the length of individual tubes. A more complete electromagnetic model would also take into account interactions between the tubes. An example approximate simulation is given in Figure 14 (black curve). It is clear that the resonances have been smoothed out. Figure 14 also shows two cases simulated for the 1 μm long device with an estimated 5 parallel tubes. We assume two values of the CNT resistance, per tube, 2 kΩ (based on [21]; red curve), and 5 kΩ (upper range based on Table I; blue curve). In this case there are clearly defined resonances. If we change v_P to be

equal to v_F, as measured in [10], the resonances shift to lower frequencies (see inset). Note that the interactions within the bundles will shift the resonance frequencies up somewhat [19] but the basic pattern should look similar. Future measurements on such short devices at several laser frequencies appear promising for distinguishing between the presently available models. For device B2 we assume a very conservative estimate of the average mismatch loss of 12 dB.

The mismatch loss is significant in many cases, but a substantial portion of the THz power is indeed typically predicted to be absorbed, partly due to the fact that the contact resistance is shunted away. For device B2, very small ripple with frequency is predicted, consistent with the measured data in Figure 12. The slow decline of S_V with frequency, evident in Figure 12. may be due to a decrease in the efficiency of the antenna. We may speculate that the higher responsivity measured at 2.54 THz is caused by a different mechanism of THz absorption. It is well-known that many CNTs are quasi-metallic (qm-SWCNTs) and have bandgaps corresponding to frequencies of 2.5 to 10 THz [26]; this may provide a second mechanism for more efficient terahertz absorption in such tubes.

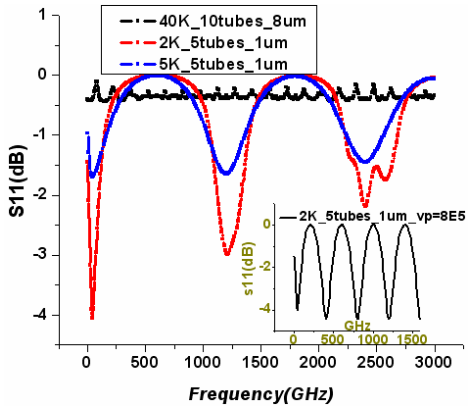

Figure 14. Simulated reflection loss (S11 in dB) between the CNT device and the LPA antenna. The devices modelled are 1) 10 tubes in parallel, 8μm long, R_{CNT} = 40 kΩ per tube (black); 2) 5 tubes in parallel, 1 μm long, R_{CNT} = 2 kΩ per tube, v_P and Z_C from [17] (red); 3) Same as 2 but R_{CNT} = 5 kΩ (blue). 4) **Inset:** 5 tubes in parallel, 1 μm long, R_{CNT} = 2 kΩ, $v_P = 8*10^5$ m/s (as in [10]) and Z_C = 12.9/4 = 3.2 kΩ.

Given that THz power is predicted to be absorbed in the m-SWCNTs, the devices would act as THz bolometers, provided that they have a sufficiently high value for the factor 'b' in Eq. (3). To investigate this, we measured IV-curves at a number of temperatures, from 4.2 K to 300 K, and calculated R and b from these, as a function of bias voltage, V_B, see Figures 15 and 16. We find that there is a maximum for $|b|$ close to T = 20 K. Also, $|b|$ decreases as the bias voltage increases. This gives rise to a characteristic signature of the bolometer process that we might look for in the responsivity data. We therefore plotted Eq. (3) while using G_{th} as an adjustable parameter to obtain best fits to the experimental data.

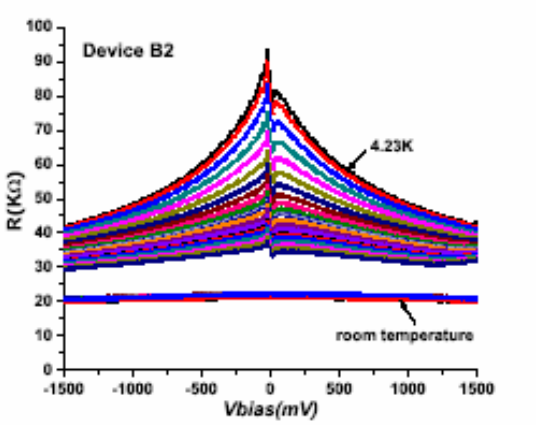

Figure 15. Resistance of device B2 versus bias voltage at a number of temperatures.

We obtained good fits in all cases independent of frequency and for temperatures up to 150 K (Figure 17). Figure 17 also demonstrates that the diode model does not produce a good fit to the measured data for this temperature range. We thus have good evidence to claim that our devices detect THz radiation based on a bolometric process at these temperatures. At 300 K the nonlinearity of the IV-curves is very small, and it is difficult to distinguish predictions based on the two models.

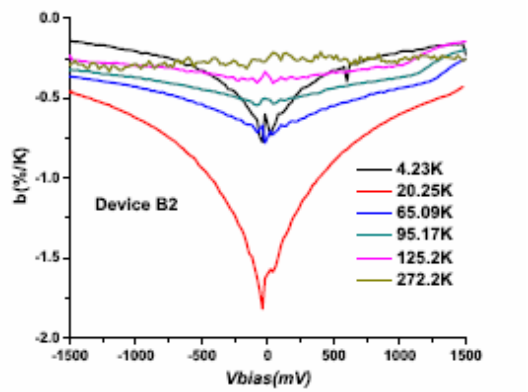

Figure 16. The temperature dependence factor b for device B2 as a function of bias voltage at different temperatures (only selected curves shown).

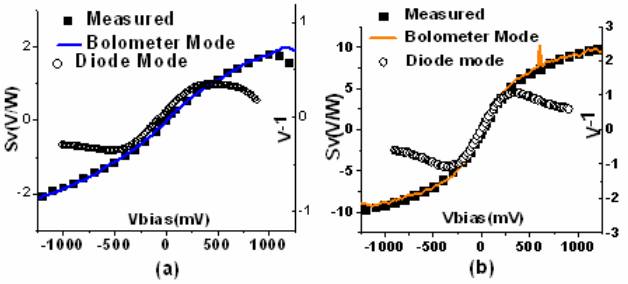

Figure 17. Best fits of Eq. (3) ('bolometer model') to the measured curves of S_V versus bias voltage. We also show predictions based on the diode model (Eq's (1) and (2)). (a) a laser frequency of 1.395 THz at 77 K and (b) a laser frequency of 0.694 THz at 4.2 K;

Some typical values of G_{th} are given in Table III.

TABLE III.

Temp. (K)	Frequ. (THz)	Gth(W/K)	Gth(W/K) (corrected)[2]
4.2	0.694	$2.33*10^{-4}$	$5.8*10^{-6}$
4.2	1.05	$3.1*10^{-4}$	$8*10^{-6}$
4.2	1.63	$6.75*10^{-4}$	$1.6*10^{-5}$
4.2	2.54	$2.76*10^{-4}$	$7*10^{-6}$
77	1.40	$2.13*10^{-3}$	$5*10^{-5}$

By measuring S_V as a function of temperature at a given bias voltage (Figure 18) we can plot G_{th} versus temperature, see Figure 19. We note that S_V decreases relatively slowly as the temperature is increased from 4.2 K, changing by a factor of two at about 25 K. This indicates a potential for this detector to work at temperatures considerably higher than LHe temperature. This feature is a result of the temperature sensitivity ($\left|\frac{db}{dT}\right|$) increasing from 4.2 K to 20 K (Figure 16), which counteracts the roughly linear increase of G_{th} with temperature up to about 100 K (Figure 19).

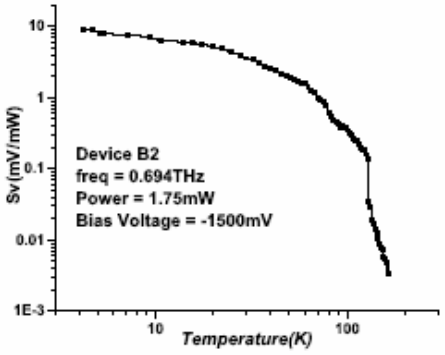

Figure 18. S_V versus temperature for Device B2 at $f_{THz} = 0.694$ THz.

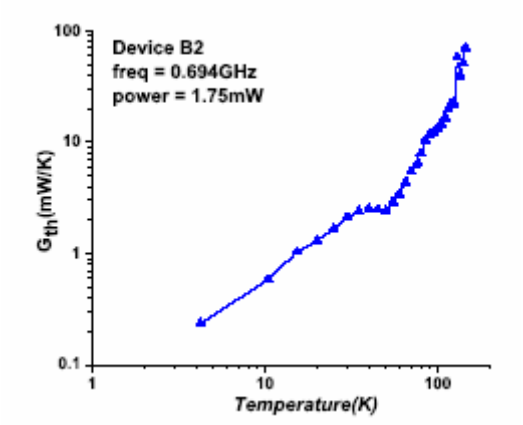

Figure 19. G_{th} versus temperature for Device B2 at $f_{THz} = 0.694$ THz.

[2] See discussion in Sec. IV.D.

D. Comparison with Thermal Conductance Theory

We can estimate G_{th} as follows: Recent work by E. Pop et al. [27,28] and Maune et al. [29] has analysed the electrical break-down for carbon nanotubes, that is known to occur at a specific temperature, about 600 °C. The power dissipation can then be correlated with the temperature, and a value derived for the thermal conductance both directly from the SWNT to the substrate (g), as well as through the contacts (G_{cont}), as pictured in Figure 20.

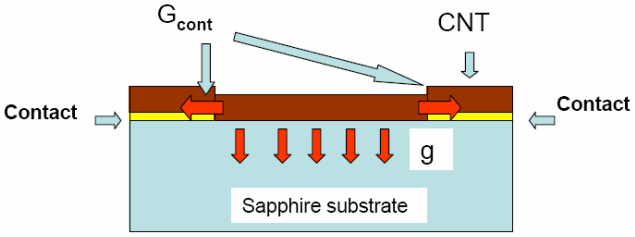

Figure 20. Illustration of heat conduction processes in the CNTs

Except for extremely short tubes, the first term (g) dominates. Further, the value of g is essentially independent of the type of substrate, indicating that the bottle neck for the process is right at the SWNT/substrate interface. From ref. [28] we can adopt an average value (for a single tube) of g = 0.15 W/mK and $G_{cont} = 8*10^{-8}$ W/K. Since these values were inferred from electrical break-down data, they apply to a situation in which the SWCNT temperature is 600 °C and the substrate at room temperature. The temperature has a maximum at the center of the tube, but is quite uniform due to the dominance of g over R_{cont} [27]. The length of the tubes is about 8 µm, and scaling from the MW data we estimate that there may be 50 tubes in parallel. We have $G_{th} = 1.2*10^{-6}$ W/K for a single tube and $6*10^{-5}$ W/K for fifty tubes in parallel. We have neglected G_{cont} . According to Prasher [30] the conductance for ballistic transport of phonons through a nano-constriction is proportional to the heat capacity. Prasher et [31] also calculate a T^4 dependence of G_{th} for a circular constriction between two (3-D) silicon half-spaces. From Ref. [32], the heat capacity for a 1-D structure is proportional to T. Although no experimental data are available to verify this yet, we assume that G_{th} varies linearly with temperature from about 873 K to 77 K. The temperature dependence for G_{th} that we plot in Figure 19 is close to linear up to about 100 K, consistent with this. We then find $G_{th} = 1.0*10^{-7}$ at 77 K for an 8 µm long m-SWCNT. The value for fifty parallel tubes is $G_{th} = 5.0*10^{-6}$ W/K. The value we estimated for G_{th} from measurements at 77 K (see Table III) is $2*10^{-3}$ W/K, however.

Here we should first note that the fits for $S_V(V_{bias})$ in Figure 17 assume that the responsivity is based on *the THz power outside the dewar*. There are known optical losses (L_{opt}) of 3-4 dB from the dewar window, a heat shield inside the dewar, and the silicon lens. Also, we estimated a mismatch loss between the antenna and the device (L_{mism}) of roughly 12 dB in Sec. IV.C. Taking these losses into account

we can modify equation (3) to yield the intrinsic responsivity based on the actual absorbed THz power:

$$S_V^{(1)} = \Delta V / P_{THz,abs} = \frac{V_0 * b}{[G_{th} + i\omega C]} \left[\frac{\eta}{L_{opt} L_{mism}} \right] (V/W) \quad (4)$$

This is the quantity that should be compared with measurement. We have introduced a further efficiency (η) which expresses the effectiveness of the (actual absorbed) THz power in changing the resistance. The estimated THz losses decrease the intrinsic responsivity by a factor of about 40 (16 dB), which adjusts the values of G_{th} in Table III by the same factor (the fourth column). At 77 K the corrected G_{th} is $5*10^{-5}$ W/K and the estimated value based on ref. [27-29] is $5*10^{-6}$ W/K, with a discrepancy of 10 dB. Possible reasons for the remaining discrepancy are:

(i) The estimate of L_{mism} is clearly very approximate.
(ii) The estimate of the number of parallel tubes is inaccurate.
(iii) Losses which can be described by the factor η. For example, the bundles contain many tubes that are "inactive" that don't change their resistance. THz power may be lost from the "active" tubes to the "inactive" ones.
(iv) The thermal conductance g [27-29] is only known at the break-down temperature. It is also not known for bundles. Plots such as Figure 19 should be useful for comparisons with extensions of the theory given in ref. [30-32]. Measurements on single tubes would be most useful for this.

We can estimate the thermal time-constant of the THz bolometer through the equation given after Eq. (3). The (total) heat capacity (C_h) was calculated based on ref [33,34]. At 77 K we find $\tau_{TH} \sim 2.5*10^{-17}/5*10^{-5} = 5*10^{-13}$ sec. which is exceedingly fast. If we take into account the extra losses represented by η, then τ_{TH} will lengthen by a factor of 1/η (10 dB) and a value of 5 ps is obtained (IF bandwidth = 32 GHz in heterodyne operation). In our experiments we found that the responsivity fell quickly above a laser modulation frequency of about 5-10 kHz. This can be explained as due to the maximum rate at which the THz gas laser could be modulated. We verified this by using a Schottky diode detector. The data in Figure 12 for devices that use antenna LPA2 are more preliminary, but we note that at 77 K device 1umB2 that used LPA2 has about an order-of-magnitude larger S_V than device B2 (with LPA1) at the same temperature. A larger responsivity may be explained because LPA2 is expected to be more efficient than LPA1. Also, the tubes are eight times shorter and thus have lower G_{th} which translates to larger S_V. The mismatch loss may also be lower. Device 1μmC3 had an almost ohmic IV-curve, and is expected to have a lower responsivity than 1μmB2, as observed.

D. Summary of the Detection Process

A brief summary of the hypothesized bolometric detection process can be given as follows:

THz radiation is absorbed in the SWCNTs proper (i.e. not in the contacts) and heats the tubes. We know from measuring R(T) that the dc resistance of the devices depends on T, which we assume is due to temperature-dependent tunnelling through the contacts (in agreement with ref. [16] and many other references). Similarly, as the SWCNTs are heated by the absorbed THz power, electron tunnelling through the contacts increases, explaining the positive increment in current that we measured. We note that, especially for the 8 μm long tubes, scattering may prevent some heated electrons from reaching the contacts. This could constitute a process that explains a decrease of the efficiency factor η in Eq. (4). **We also note that while the expressions for the "diode" process occurring at MW (Equ's (1)-(2)) and the THz bolometric process (Equ's (3)-(4)) are different, they both ultimately rely on the electron tunnelling process through the contact barriers.**

V. LARGE-SCALE AB INITIO SIMULATION

In order to obtain the different component characteristics presented in the equivalent circuit model in Fig.4, we aim to go beyond the current state-of-art capabilities for simulating CNTs by developing large-scale *ab-initio* atomistic approaches. Our proposed atomistic Density Functional Theory (DFT) and Kohn-Sham equation approach has the potential to clear up our understanding of many experimental issues, and to offer the high degree of reliability and accuracy needed to characterize the following macroscopic quantities: kinetic inductance, contact resistance and contact capacitance, quantum capacitance and CNT resistance.

Because of their high consumption of computational resources, *ab-initio* electronic structure and transport calculations are usually limited to either small molecular systems [35,36], or isolated regions of the carbon nanotube close to the metal contacts or possible defects [37,38]. An *ab-initio* atomistic description of a long CNT up to 100nm (~ 10,000 atoms), which has been so far considered as a formidable task, could however provide important insights into the electronic properties of the device. In order to achieve this goal efficiently, we have been developing innovative numerical modeling strategies using a real-space mesh technique framework and a combination of mathematical methodologies and high-performance parallel algorithms [39] (mode approach/contour integration/ efficient banded solver). To give a perspective of the computational time required by our proposed atomistic-based simulation, only a few minutes of CPU time are needed to obtain electronic properties (electron density, potential, etc.) of long nanotubes which is order of magnitude faster than any other existing *ab-initio* techniques (see Fig. 21).

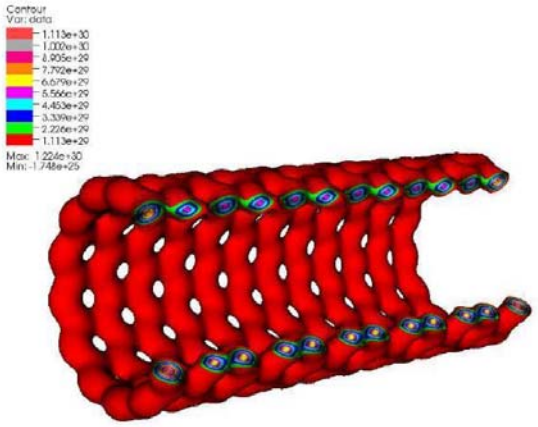

Figure 21. Electron density in CNT calculated using real-space pseudopotentials.

The approach is also highly scalable using the parallel SPIKE solver [40,41]. In addition it can be adapted to perform time dependent DFT calculations by solving the Kohn-Sham equations using a Crank Nicolson scheme and by adapting the transient simulation approach proposed in [42]. Since the terahertz experimental data may be altered by defects, vacancies, charge impurities, and other distortions, we have shown that our numerical approach can be used to study as well the device characteristics response to these different excitations [39].

In practice, the DFT-Kohn-Sham equation can be used in association with accurate pseudopotentials to remove the core electrons, and the local density approximation (LDA) to account for the many-body exchange-correlations term. However, since the effect of core electrons in CNT may not be negligible [43], we have very recently successfully performed all-electron calculations and obtained preliminary results [44].

VI. DISCUSSION AND CONCLUSIONS

In this paper we have described measurements of improved MW detection in bundles of SWCNTs, compared with our previous results [3,4] (response to higher frequencies, larger responsivity). MW ANA measurements also resulted in an equivalent circuit model, valid to 26 GHz. Devices were rapidly fabricated by DEP by which several parallel bundles were placed on contacts. The circuit model demonstrates that substantial (4 – 40 fF) capacitance exists parallel to the contact resistance.

We have demonstrated the first detection of terahertz radiation (up to 2.54 THz) in bundles of m-SWNT devices. We employed quasi-optical coupling with a silicon lens and log-periodic antennas, a technology taken over from our previous NbN HEB work, well familiar to participants in the ISSTT symposia. So far, the maximum voltage responsivity measured is about 16 V/W (30-40 V/W at the antenna terminals), at 77 K (that device is expected to have had a much larger S_V at 4.2 K). The temperature dependence of S_V is quite gradual up to about 50 K indicating a potential for operation well above 4.2 K. While the responsivity is not very large at this state of the development, we note that another recent (fast) quasi-optical THz detector using Schottky diodes [45] had a similar responsivity.

We explain the detection process in the new THz detector as being bolometric, which agrees with our detailed measurements and modelling. The detector resembles phonon-cooled NbN HEBs in that the main heat conduction mechanism is directly from the active element to the substrate. The thermal conduction process is known to be very strong [27-29] which is one aspect that limits the present responsivity. It should be straight-forward to modify the devices by etching a trench in an oxidized high-ρ silicon substrate, or in the silicon layer of an SOS susbstrate, and suspend the SWNTs across this trench, as has been demonstrated in many other experiments (ref. [27] and references given there; also [46]). The thermal conductance will be *along* the tubes in this case, and considerably lower, which will increase the responsivity. It is useful to compare ref. [11] which achieved $S_V \sim 1{,}000$ V/W in the Near IR (that bolometer has a much larger heat capacity and thus longer time constant). We plan to fabricate suspended SWCNT devices, which will also help further verify the bolometric model. Note that this version of the CNT detector will then be similar to a diffusion cooled HEB [47], and also similar to the ballistic cooling HEB of M. Lee et al. [48].

Another potential area for improvement is the optical coupling. While the use of bundles of tubes, and cancellation of the effect of the contact resistance at THz, are useful features that we have demonstrated, full optimization may eventually require some type of matching transformer [1].

Based on the low heat capacity and large thermal conductance of the new devices we predict a very short thermal time-constant (~ 5 ps). Much shorter time constants should be feasible for the suspended CNT version. In the ballistic limit, assuming electron cooling [1,2]:

$$\tau_{TH} \sim 1.25 \text{ ps} * (L(\mu m)) \qquad (5)$$

Here we have set the electron velocity equal to the Fermi velocity ($8.1*10^7$ cm/s). If plasmon phenomena dominate the THz transport (see Sec. III.A) even shorter time constants are predicted. Of course, such predictions must be verified through future work. We plan to develop a heterodyne detector, which will eventually allow us to measure the IF bandwidth, and thus verify the thermal time-constant. Finally, it is expected that the performance of the detector can be extended to frequencies well above 2.5 THz. Clearly, much work still lies ahead, but that work can now build on the concrete results described above.

ACKNOWLEDGMENT

This work was supported by NSF grants ECS-0508436 and ECS-0725613.

REFERENCES

[1] K.S. Yngvesson, "A New Hot Electron Bolometer Heterodyne Detector Based on Single-Walled Carbon Nanotubes," *16th Intern. Symp. Space Terahertz Technol.*, Gőteborg, Sweden, May 2005, p. 531.

[2] K.S. Yngvesson, "Very wide bandwidth hot electron bolometer heterodyne detectors based on single-walled carbon nanotubes," *Applied Phys. Lett,* vol. **87**, p. 043503 (2005).

[3] K.S. Yngvesson, F. Rodriguez-Morales, R. Zannoni, J. Nicholson, M. Fishetti, and J. Appenzeller, "Microwave Detection and Mixing in Metallic Single Wall Carbon Nanotubes and Potential for a New Terahertz Detector," *17th Intern. Symp. Space Terahertz Technol.*, Paris, France, May 2006, p. 135.

[4] F. Rodriguez-Morales, R. Zannoni, J. Nicholson, M. Fischetti, K. S. Yngvesson, and J. Appenzeller, *Appl. Phys. Lett*. **89**, 083502 _2006_.

[5] H.M. Manohara, E.W. Wong, E. Schlecht, B.D. Hunt, and P.H. Siegel, *Nano Lett.* **5**, 1469 (2005).

[6] S. Rosenblatt, H. Lin, V. Sazonova, S. Tiwari, and P.L. McEuen, *Appl. Phys. Lett*. **87**, 153111 (2005).

[7] A. A. Pesetski, J.E. Baumgardner, E. Folk, J. Przybysz, J. D. Adam, and H. Zhang, *Appl. Phys. Lett.*, **88**, 113103 (2006).

[8] M. Tarasov, J. Svensson, L. Kuzmin, and E. E. B. Campbell, *Appl.Phys.Lett.*, **90**, 163503 (2007).

[9] C. Rutherglen and P. Burke, "Carbon Nanotube Radio," *Nano Letters*, **7**, p. 3296 (2007).

[10] Z. Zhong, N.M. Gabor, J.E. Sharping, A.L. Gaeta, and P.L. McEuen, "Terahertz time-domain measurement of ballistic electron resonance in a single-walled carbon nanotube," *Nature Nanotechnol.* **3**, 201 (2008).

[11] M.E. Itkis, F. Borondics, A. Yu and R.C. Haddon, *Science,* **312**, 413 (2006).

[12] K. Fu, R. Zannoni, C. Chan, S.H.Adams, J. Nicholson, E. Polizzi and K.S. Yngvesson, "Terahertz detection in single wall carbon nanotubes," *Appl. Phys. Lett.*, **92**, 033105 (2008).

[13] K. Fu, "Metallic Carbon Nanotubes, Microwave Characterization and Development of a Terahertz Detector," *M.Sc. thesis, University of Massachusetts, Amherst, MA* (2008).

[14] R. Krupke and F. Hennrich, *Adv. Eng. Mater.* **7**, 111 _2005.

[15] Cheap Tubes, Brattleboro, Vt.. Purified 90% SWCNTs, grown by CVD, nominal diameter from 1 to 2 nm., average length of 50 μm before ultrasonication.

[16] Z. Yao, C.L. Kane, and C. Dekker, *Phys. Rev. Lett.* **84**, 2941 (2000).

[17] P. J. Burke, "Lüttinger liquid theory as a model of the gigahertz electrical properties of carbon nanotubes," *IEEE Trans. Nanotech*. **1**, 129 (2002).

[18] G.W. Hanson, "Fundamental Transmitting Properties of Carbon Nanotube Antennas", *IEEE Trans. Antennas Propagat.*, **53,** 2426 (2005).

[19] M. V. Shuba, S. A. Maksimenko and A. Lakhtakia "Electromagnetic wave propagation in an almost circular bundle of closely packed metallic carbon nanotubes" *Phys. Rev. B*., **76,** 155407 (2007).

[20] M. S. Purewal, B. H. Hong, A. Ravi, B. Chandra, J. Hone, and P. Kim, "Scaling of Resistance and Electron Mean Free Path of Single-Walled Carbon Nanotubes", *Phys.Rev.Lett*. **98**, 186808 (2007).

[21] J. J. Plombon, K. P. O'Brien, F. Gstrein, V. M. Dubin, and Y. Jiao, High-Frequency Electrical Properties of Individual and Bundled Carbon Nanotubes," *Appl. Phys. Lett.* **90**, 063106 (2007).

[22] M. Zhang, X. Huo, P. C. H. Chan, Q. Liang, and Z. K. Tang, "Radio-frequency transmission properties of carbon nanotubes in a field-effect transistor configuration," *IEEE Electron Device Letters*, **27**, p. 668, Aug. 2006.

[23] K.S. Yngvesson, "*Microwave Semiconductor Devices*", Kluwer Academic, Norwell, MA (1991).

[24] E. Gerecht, C. Musante, Y. Zhuang, K. Yngvesson, T. Goyette, J. Dickinson, J. Waldman, P. Yagoubov, G. Gol'tsman, B. Voronov, and E. Gershenzon, *IEEE Trans. Microwave Theory Techn.*, vol. **47**, pp. 2519–2527, (1999).

[25] P.L. Richards, *J. Appl. Phys*., **76**, 1 (1994).

[26] M. Itkis, S. Niyogi, M.E. Meng, H. Hu and R.C. Haddon, *Nanolett.* **2**, 155 (2002).

[27] E. Pop, D.A. Mann, K. Goodson, and H. Dai, J. Appl. Phys., **101**, 093710 (2007). Also see references therein.

[28] E. Pop, "The role of Electrical and Thermal Contact Resistance for Joule Breakdown of Single-Wall Carbon Nanotubes," to appear in *Nanotechnology* (2008). Available at *arXiv-condmat* 0805.1937.

[29] H. Maune, H.-Y. Chiu and M. Bockrath., *Appl. Phys. Lett.*, **83**, 013109 (2006).

[30] R. Prasher, *Nanolett*. **5**, 2155 (2005).

[31] R. Prasher, T. Tong and A. Majumdar, *Appl. Phys. Lett.* **91**, 143119 (2007).

[32] J. Hone, B. Batlogg, Z. Benes, A. T. Johnson, J. E. Fischer, "Quantized Phonon Spectrum of Single-Wall Carbon Nanotubes", *Science*, **289**,1730 (2000).

[33] P. L. McEuen, in C. Kittel, *Introduction to Solid State Physics*, Eighth Ed., Wiley, 2005, Chapter **18**.

[34] C. Yu, L. Shi, Z. Yao, D. Li and A. Majumdar, *Nanolett*. 5, 1842 (2005)

[35] M. Brandbyge, J-L Mozos, P Ordejon, J. Taylor, and K. Stokbro. *"Density-functional method for nonequilibrium electron transport", Phys. Rev B*, **65**, 165401 (2002).

[36] A. Garcia-Lekue, L-W. Wang "Elastic quantum transport calculations for molecular nano devices using plane waves", *Phys. Rev. B* **74,** 245404 (2006)

[37] H. J. Choi, J. Ihm, "Ab initio pseudopotential method for the calculation of conductance in quantum wires", *Phys. Rev. B,* **59**, 3 pp 2267-2275 (1998)

[38] W. Zhu, E. Kaxiras, "Schottky barrier formation at a carbon nanotube- metal junction", *Appl. Phys. Lett.* **89**, 243107 (2006)

[39] D. Zhang and E. Polizzi, "Efficient Modeling Techniques for Atomistic-Based Electronic Density Calculations", *J. Comp. Elec.* (in press, 2008).

[40] E. Polizzi, A. Sameh. "A Parallel Hybrid Banded System Solver: The SPIKE Algorithm", *Parallel Computing*, **32**, 2, pp. 177-194 (2006).

[41] SPIKE has been released in: http://whait.intel.com

[42] O. Pinaud, "Transcient simulations of resonant tunneling diode", *J. Appl. Phys.* **92**,1 p1987 (2002).

[43] Y. Kawazoe, K. Ohno, K. Esfarjani, Y. Maruyama, K. Shiga and A. Farajian, *"Why the all-electron full-potential approach is suitable for calculations on fullerenes and nanotubes? ", J. of Molecular Graphics and Modelling* **19**, Issue 2, pp 270-273, (2001).

[44] E. Polizzi, (unpublished, 2008).

[45] T. Yasui, A. Nishimura, T. Suzuki, K. Nakayama, and S. Okajima, "Detection system operating at up to 7 THz using quasioptics and Schottky barrier diodes," *Rev. Sci Instrum*. **77,** 066102 (2006).

[46] J. Cao, Q. Wang, D. Wang and H. Dai, "*Suspended Carbon Nanotube Quantum Wires with Two Gates*", Small, **1**, 138 (2005).

[47] D. Prober, "Superconducting Terahertz mixer using a transition-edge microbolometer," *Appl. Phys. Lett.* **62,** 2119 (1993).

[48] M. Lee, L.N. Pfeiffer and K. West, "Ballistic Cooling in a Wide-Band Two-Dimensional Electron Gas Bolometric Mixer", *Appl. Phys. Lett.* **81**, 1243 (2002).